Springer

KSME

Journal of Mechanical Science and Technology 25 (8) (2011) 1885~1892
www.springerlink.com/content/1738-494x
DOI 10.1007/s12206-011-0516-7

Experimental investigation and performance analysis of a dual-cylinder opposed linear compressor †

Huiming Zou[1,*], Liqin Zhang[1,2], Guohong Peng[1,2] and Changqing Tian[1]

[1]*Technical Institute of Physics and Chemistry, Chinese Academy of Sciences, Beijing 100190, China*
[2]*Graduate University of Chinese Academy of Sciences, Beijing 100190, China*

(Manuscript Received October 26, 2010; Revised March 2, 2011; Accepted April 20, 2011)

Abstract

The dual-cylinder opposed linear compressor (DOLC) contains a couple of symmetrical gas loads on the two sides of the movement components. Because the gas loads are symmetrical, the balanced position of movement components will not be offset by gas force during the operating process, and piston displacement can be detected and controlled more easily. Based on the kinetics and thermodynamics theory, the non-linear gas load of the DOLC was linearized by the Fourier method. The relationship between the supply voltage and displacement is presented. Through air compression experiments, the operation features of the DOLC with different syntonic spring groups were analyzed. The performance of the DOLC was considerably affected by work conditions and the stiffness of syntonic spring groups; the closer the work condition was to the sympathetic vibration, the higher the observed efficiency of the DOLC. A jump, hysteresis, and an unstable phenomenon in the process of voltage regulation occurred around sympathetic vibration conditions. In the process of increasing voltage on a certain discharge pressure condition, the displacement jump phenomenon occurred when the intrinsic frequency approacheds power frequency, causing the discharge pressure to drop synchronously. In the process of decreasing voltage on the lower discharge pressure condition, the displacement shrink phenomenon occurred when the intrinsic frequency approached power frequency. Because sympathetic vibration conditions changed with discharge pressures, a hysteresis district existed between the displacement jump point and shrink point. The DOLC worked unstably on the hysteresis district because the discharge pressure fluctuated between the two values. To make the DOLC work stably on higher efficiency, the intrinsic frequency should be configured to a slightly larger value than the power frequency by setting the syntonic spring groups and the mass of movement components to the ratings on the work conditions. Controlling the power frequency after is needed to adhere to the intrinsic frequency of the variable work conditions.

Keywords: Linear compressor; Dual-cylinder; Dynamics characteristics; Sympathetic vibration

1. Introduction

Developed from the earlier application on cryocoolers, linear compressors are being increasingly applied in the civil field, particularly on household refrigerators and portable coolers. The main advantages of the linear compressor are its high efficiency and compact structure, which eliminate the need for a conversion mechanism to transform rotary motion into reciprocating motion. The dynamic characteristics of linear compressor have been investigated by many scholars; the main type of linear compressor investigated and applied popularly is the single-cylinder type. Minas [1] created a mathematical model of the linear compressor, analyzed the nonlinear dynamic characteristics of an oilless linear compressor, and proposed that the optimal frequency of a linear compressor is dependent on mass flux. Choe and Kim [2, 3] studied the frequency response characteristics and jump phenomenon of the linear compressor by simplifying the gas force into linear force using numerical analysis. Lamantia et al. [4] analyzed the dynamic characteristics and optimized the total performance of a linear compressor based on Simulink and Adams. N. Chen et al. [5] studied the static and dynamic characteristics of moving-magnet linear compressors in Stirling and pulse tube cryocoolers. Hyun Kim et al. [6] analyzed the dynamic characteristics and coefficient of performance of a linear compressor in a refrigeration system with R600a refrigerant.

Compared to a single-cylinder linear compressor, the dual-cylinder opposed linear compressor (DOLC) is noteworthy because it has a couple of cylinders and pistons on the two sides of the movement components, which can be used to supply larger cooling capacity. The gas loads are symmetrical, thus the balanced position of movement components will not be offset by gas force during operation. Piston displacements

† This paper was recommended for publication in revised form by Associate Editor Cheolung Cheong

* Corresponding author. Tel.: +8601082543433, Fax.: +8682543696
E-mail address: zouhuiming77@126.com

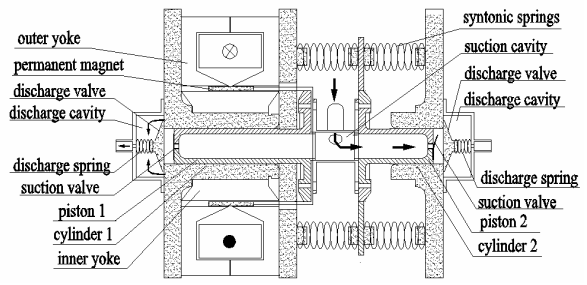

Fig. 1. Schematic diagram of the DOLC.

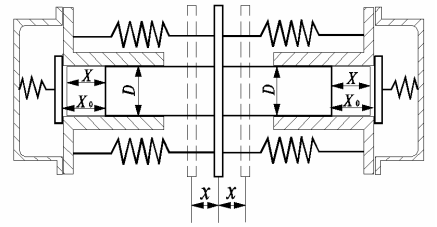

Fig. 2. Kinetic model of the DOLC.

are easier to detect and control and the two cylinders of the DOLC can be used to deal with work fluid under different work conditions. This provides the DOLC a wider application to meet mutative demands. However, reports on the performance and application of DOLC are limited particularly on its actual performance under different work conditions. The present paper developed a DOLC with symmetrical gas loads and analyzed their performances through air compression experiments.

2. Principle and mathematics model of the DOLC

Fig. 1 shows the schematic diagram of the DOLC. The driver of the DOLC is a moving-magnet linear oscillation motor composed of an outer yoke, inner yoke, coil, and permanent magnet. Permanent magnet, suction cavity, and two opposed pistons form the mover of linear motor, and syntonic springs are set between the mover and framework. Two opposed pistons are installed separately in two cylinders, and two suction valves are likewise installed separately on at the head face of the pistons. On At the end surface of each cylinder, there is a discharge cavity containing a discharge valve and discharge spring. The discharge valve is pre-pressurized to contact with the cylinder end surface by the discharge spring.

Fig. 2 shows the kinetic model of the DOLC, where D is the diameter of the cylinders, X is the amplitude of piston displacement, X_0 is the clearance distance, and x is the piston displacement that can be expressed by $x = X\sin\omega t$.

The kinetic mathematical model of the DOLC can be expressed by:

$$m\frac{d^2x}{dt^2} + c_f\frac{dx}{dt} + k_s x + F_g = F_e \tag{1}$$

where m is the mover mass, c_f is the friction damping coefficient, k_s is the stiffness coefficient of syntonic springs, F_g is the gas force, and F_e is the electromagnetic force, which can be expressed as $F_e = K_0 i$ (K_0 is electromagnetic force coefficient and i is the current) [7].

As the mover of DOLC moves to one side, the piston on this side begins to compress the gas, and the discharge valve on this side opens to discharge the gas once the pressure inside the cylinder is higher than the discharge pressure. At the opposite side, the suction valve opens to inhale the gas. In the actual work cycle of the reciprocating compressor, heat transfer and flow leakage that are both difficult to calculate accurately exist. To simplify the mathematical model of gas force, compression and expansion processes of the actual cycle are generally regarded as constant-quality polytropic processes. The mathematical models of gas force are shown in the appendix.

Incorporating the linearized gas force shown in the appendix into Eq. (1), the kinetic mathematical model of the DOLC can be expressed by Eq. (2), in which the first part is inertial force, the second part is damping force, the third part is elastic force, and the last part is electromagnetic force.

$$m\frac{d^2x}{dt^2} + \left(c_f + c_g\right)\frac{dx}{dt} + \left(k_s + k_g\right)x = K_0 i \tag{2}$$

where c_g is the gas equivalent damping coefficient and k_g is the gas equivalent stiffness coefficient.

The electromagnetic field of the moving-magnet linear motor can be analyzed by the equivalent magnetic model. The electromagnetic mathematical model of DOLC can be expressed as:

$$u = iR_e + L_e\frac{di}{dt} + K_0\frac{dx}{dt} \tag{3}$$

where u is the voltage, i is the current, R_e is the equivalent resistance, and L_e is the equivalent inductance [2].

Putting $x = X\sin\omega t$ into Eq. (3),

$$i = \frac{1}{K_0}\left[-m\omega^2 X\sin\omega t + \left(c_f + c_g\right)\omega X\cos\omega t + \left(k_s + k_g\right)X\sin\omega t\right]. \tag{4}$$

Incorporating Eq. (4) into Eq. (3),

$$\begin{aligned} u = {} & \frac{R_e}{K_0}\left[-m\omega^2 X\sin\omega t + \left(c_f + c_g\right)\omega X\cos\omega t + \left(k_s + k_g\right)X\sin\omega t\right] \\ & + \frac{L_e}{K_0}\left[-m\omega^3 X\cos\omega t - \left(c_f + c_g\right)\omega^2 X\sin\omega t + \left(k_s + k_g\right)\omega X\cos\omega t\right] \\ & + K_0\omega X\cos\omega t. \end{aligned} \tag{5}$$

The phase angle θ between voltage u and current i can be expressed as:

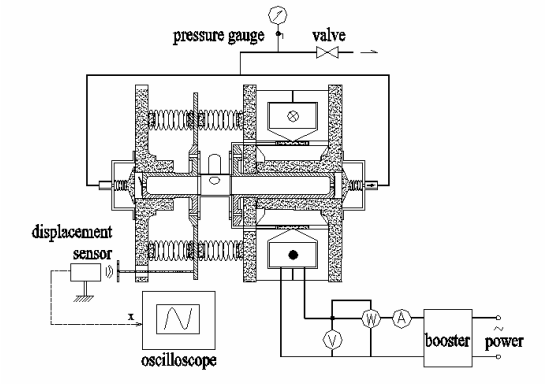

(a)

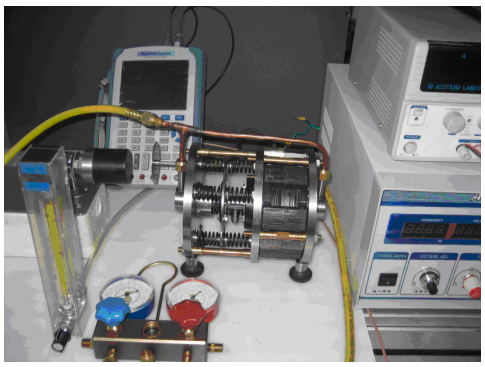

(b)

Fig. 3. Experimental system: (a) schematic diagram; (b) photo.

$$\theta = \arctan\frac{\omega\left(c_f + c_g\right)}{-m\omega^2 + k_s + k_g} - \arctan\frac{\left[R_e\omega\left(c_f + c_g\right) + L_e\omega\left(-m\omega^2 + k_s + k_g\right) + K_0{}^2\omega\right]}{R_e\left(-m\omega^2 + k_s + k_g\right) - L_e\omega^2\left(c_f + c_g\right)}. \quad (6)$$

The effective current, effective voltage, and input power can be expressed as:

$$I = \frac{\sqrt{2}X}{2K_0}\left\{\left(-m\omega^2 + k_s + k_g\right)^2 + \left[\omega\left(c_f + c_g\right)\right]^2\right\}^{0.5} \quad (7)$$

$$U = \frac{\sqrt{2}X}{2K_0}\left\{\begin{array}{l}\left[R_e\left(-m\omega^2 + k_s + k_g\right) - L_e\omega^2\left(c_f + c_g\right)\right]^2 + \\ \left[R_e\omega\left(c_f + c_g\right) + L_e\omega\left(-m\omega^2 + k_s + k_g\right) + K_0{}^2\omega\right]^2\end{array}\right\}^{0.5} \quad (8)$$

$$P_i = \frac{2\pi}{\omega}\int_0^T iudt = UI\cos\theta. \quad (9)$$

The output power and efficiency can be expressed as:

$$P_o = \frac{1}{2}c_g(\omega X)^2 \quad (10)$$

$$\eta = \frac{P_o}{P_i}. \quad (11)$$

Table 1. Basic parameters of the tested compressor.

Items	Unit	Values
Operating frequency, f	Hz	50
Magnet force coefficient, K_0	N/A	69
Equivalent resistance, R_e	Ω	15.85
Equivalent inductance, L_e	H	0.42
Mover mass, m	kg	0.706
Cylinder diameter, D	mm	20
Initial clearance distance, X_0	mm	5.75

3. Experimental facility and procedure

The experiments used air as work fluid to test the performance of DOLC, allowing the linear compressor to operate without shell and to measure displacement conveniently and accurately. Fig. 3 shows the experimental system. The compressor stands on the experimental flat isolated by rubber cushions attached to the flat, and subsequently sucks air and discharges it back through the adjusting valve. The discharge pressure can be adjusted using the valve.

Table 1 shows the basic parameters of the developed DOLC prototype. The magnet force coefficient, equivalent resistance, and equivalent inductance were tested from the linear motor.

Power supply can be adjusted and measured by an intelligent digital booster with a function power meter. Discharge pressure p_d can be determined using a pressure gauge. The amplitude of piston displacement X can be recorded by an eddy current displacement sensor and can be shown using a digital storage oscilloscope. The experimental procedures are as follows:

(a) Operate the compressor to compress air with two different syntonic spring groups. The stiffness of No.1 spring group is 44190 N/m, and the stiffness of No. 2 spring group is 36440 N/m.

(b) Make the amplitude of piston displacement to a setting value and measure the corresponding input power on different discharge pressures.

(c) Keep the discharge pressure at a certain value, adjust the supply voltage to change the amplitude of piston displacement, and measure the corresponding input power.

(d) Calculate the output power and efficiency.

4. Results and discussion

4.1 Performance experiments on different discharge pressures

Keep the amplitude of piston displacement at 11.4 mm, increase the discharge pressure from 0.2−0.9 MPa by adjusting the booster and the valve, and measure the supply power parameters correspondingly. The suction pressure should have 0.1 MPa atmospheric pressure. Fig. 4 shows the supply power parameter curves with the increasing discharge pressures of the developed DOLC. The DOLC prototype worked with the above two kinds of spring groups. The discharge pressure was the absolute pressure, and the currents of the DOLC with two

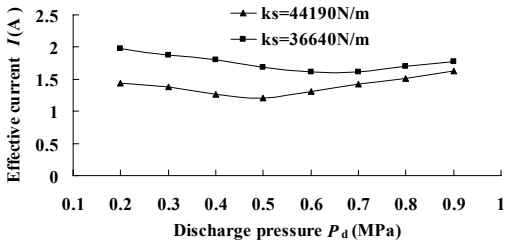

(a)

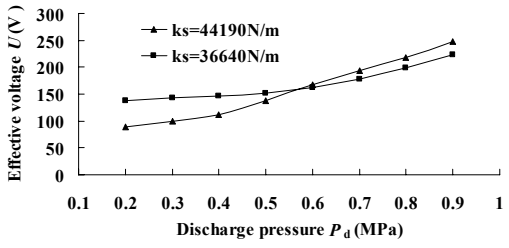

(b)

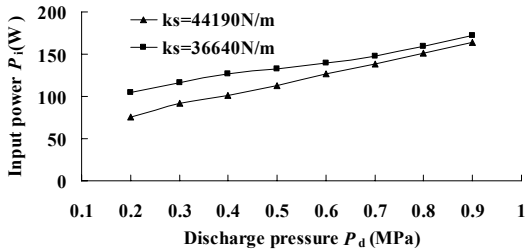

(c)

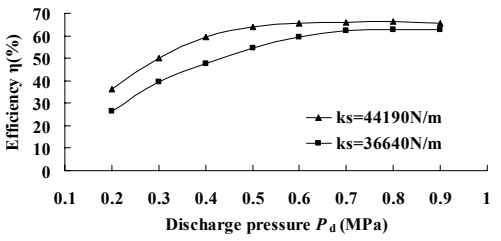

(d)

Fig. 4. Supply power parameters curves on different discharge pressures (suction pressure: 0.1 MPa): (a) effective voltage; (b) effective current; (c) input power; (d) efficiency.

different spring groups both decreased at the beginning and subsequently increased. A discharge pressure inflexion on which the current is at the lowest point was observed. The discharge pressure inflexion of the experiments with No. 1 spring group was 0.5 MPa, whereas that of the experiments with No. 2 spring group was 0.7 MPa. The voltages of the DOLC with two different spring groups increased although the rates of voltage increase were different. A certain discharge pressure value under which the voltage increase rate is lower and above which the rate is larger was observed as well. The discharge pressure value of the experiments with No. 1 spring group was 0.5 MPa, whereas that of the experiments with No. 2 spring group was 0.7 MPa. The input powers of the

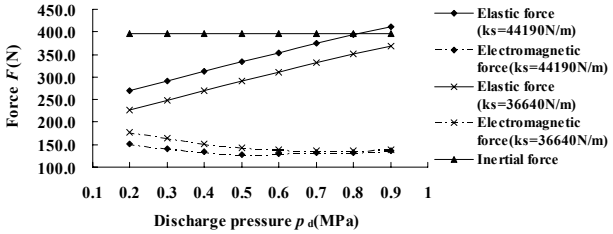

Fig. 5. Forces on different discharge pressures.

DOLC with the two different spring groups both increased with the discharge pressure. The efficiency of the DOLC with No.1 spring group increased at the beginning and subsequently decreased, with a discharge pressure of 0.8 MPa at the efficiency point. The efficiency of the DOLC with No. 2 spring group increased with the increase of the discharge pressure until 0.9 MPa.

The physical meaning of the experimental results can be explained according to the mathematical model of the DOLC. Current and electromagnetic force are related as a direct ratio. The voltage is determined by the current and angle between the current and displacement, which are both related to electromagnetic force. The electromagnetic force can be calculated according to Eq. (2) after deriving the values of the inertial forces, damping forces, and elastic forces on the respective discharge pressures of the developed DOLC prototype with 11.4 mm piston stroke. According to Eqs. (4)-(11), the efficiency will be affected by the relationship between the inertial forces and elastic forces.

Fig. 5 shows the calculated results. The electromagnetic force curves decreased and subsequently increased with discharge pressure. The discharge pressure of the developed DOLC with No.1 spring group was 0.5 MPa at the lowest point of the electromagnetic force. The discharge pressure of the developed DOLC with No. 2 spring group was 0.7 MPa. The inflexion of the calculated current and voltage agrees with the experimental results.

The elastic force curve of the developed DOLC with No. 1 spring group was larger than that of the compressor with No. 2 spring group, and closer to the inertial force curve. A cross point, the sympathetic vibration point, on the inertial and elastic force curve of the developed DOLC with No. 1 spring group was observed on the 0.8 MPa discharge pressure. The calculated results agree with the experimental results. This suggests that the highest efficiency of the DOLC with No. 1 spring group was on the 0.8 MPa discharge pressure, and that of the DOLC with No. 2 spring group was on the 0.9 MPa discharge pressure.

The performance features of the DOLC, as analyzed by the linearized kinetic mathematical model, agree well with the experimental results. The research results of the DOLC performance experiment on different discharge pressure show that:

(a) To keep the amplitude of piston displacement on the same value, the voltage and input power should be augmented

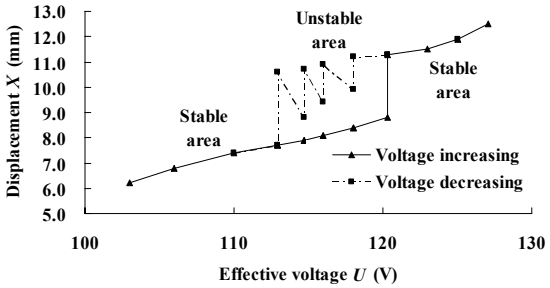

Fig. 6. Changes in the displacement curves with different voltages (suction pressure: 0.1 MPa).

with the increase in discharge pressure.

(b) The closer the elastic force is to the inertial force, the higher the efficiency.

4.2 Jump and unstable hysteresis phenomenon

Keep the developed DOLC prototype with No. 1 spring group working on a certain discharge pressure and change the amplitude of piston displacement by adjusting the supply voltage. The experimental results show that a jump, hysteresis, and an unstable phenomenon occurred in the process of voltage regulation under several conditions. Firstly, an increase in the displacement was obtained by augmenting the voltage. At the beginning, the displacement increased with the voltage stably. As the voltage attained a certain value, the displacement abruptly jumped to a larger status. Subsequently, the displacement continued to increase with the increase in voltage. Secondly, the displacement was decreased by diminishing the voltage. As the voltage decreased until it was less than the jump point, the linear compressor proceeded into an unstable status, which was maintained on a particular stage with the decrease in voltage. When the voltage decreased to another lower value, the displacement was suddenly reduced to a low status. The displacement returned to a stable status. Consequently, it decreased continually with the voltage.

Fig. 6 shows the displacement curves that changed with the voltage on 0.5 MPa discharge pressure. During the period of increasing voltage, the displacement increased stably by jumping from 8.7−11.5 mm at 120.3V, and continued to increase with the increase in voltage. During the period of decreasing voltage, the displacement decreased by proceeding into an unstable status from 120V, and subsequently decreased from 10.8−6.9 mm at 112.9V. The decrease continued further. Discharge pressure increased from 0.1−0.5 MPa with the increase of displacement, dropped to 0.38 MPa because of the jump phenomenon, and fluctuated between 0.38 and 0.5 MPa during the unstable stage.

According to the theory of mechanical vibration, as the intrinsic frequency ($\omega_n = \left[(k_s + k_g)/m\right]^{0.5}$) approximates the power frequency, that is the frequency ratio $\lambda = \omega_n / \omega \approx 1$, a very violent sympathetic vibration will occur.

The gas equivalent stiffness coefficient on different displacements of the DOLC prototype can be calculated according to the parameters in the appendix. Fig. 7 shows that the frequency ratio curves changed with the displacement of the developed DOLC prototype with No. 1 spring group on 0.38 and 0.5 MPa discharge pressure values.

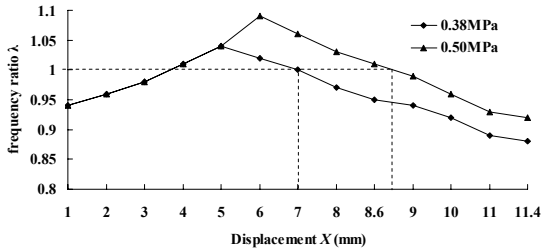

Fig. 7. Changes in frequency ratio curves with the displacement.

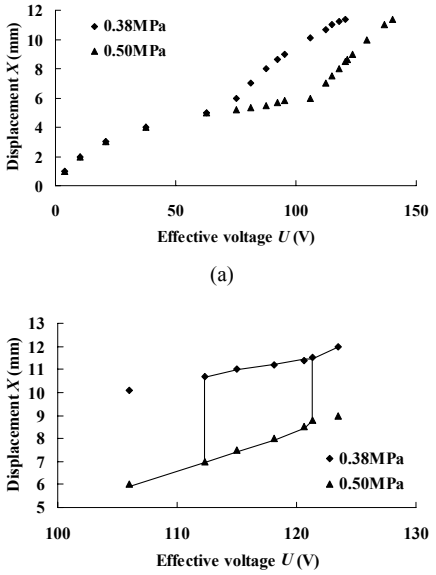

Fig. 8. Changes in the calculated displacement curves with effective voltages: (a) total plot; (b) local plot.

When the frequency ratio was λ=1, the displacement was approximately 8.8 mm on the 0.5 MPa discharge pressure and approximately 7.0mm on the 0.38 MPa discharge pressure. The intrinsic frequency increased with the increase in displacement before pumping and decreased with the increase in displacement after pumping. On the lower discharge pressure, earlier pumping happened and the intrinsic frequency was less than that of the higher discharge pressure.

Fig. 8 shows the calculated displacement changes with the effective voltage on the different displacements of the DOLC prototype as derived by Eq. (8). When the effective voltage was 121.3V, the displacement was approximately 8.8 mm on the 0.5 MPa and approximately 11.4mm on the 0.38 MPa. When the effective voltage was 112.3V, the displacement was approximately 7.0 mm on the 0.5 MPa and approximately 10.7 mm on the 0.38 MPa.

The calculated results shown in Figs. 7 and 8 are similar with the experimental results. As the voltage increased, the

displacement jump phenomenon occurred near the point where the frequency ratio was λ=1.0. The displacement jump caused the discharge pressure to drop to a lower value. As the voltage decreased, the displacement shrink phenomenon occurred near the point where the frequency ratio was λ=1.0 on the lower discharge pressure. The hysteresis was formed by the unstable district from the jump point on higher discharge pressure to the shrink point on the lower discharge pressure. This validates the observation that if the intrinsic frequency is approaching power frequency, jump, hysteresis, and an unstable phenomenon will occur. The pistons would bump the discharge valve and the gas pressure would fluctuate. To make sure that the linear compressor can work on a stable and higher efficiency status, controlling the frequency is necessary.

According to Fig. 7, the intrinsic frequency is lowest on the TDC point after pumping. If the frequency ratio is a slightly larger than 1.0 on the TDC point, the sympathetic vibration will not occur during the process of increasing displacement because the efficiency will only be slightly lower than that of the sympathetic vibration. One way to avoid sympathetic vibration is to set the syntonic spring groups and movement component mass on the rating work condition to allow the intrinsic frequency to become slightly larger than the power frequency on the TDC point.

Fig. 7 shows that the intrinsic frequency will change with the work conditions. Adjusting the power and intrinsic frequency on variable work conditions through the control system will maintain the smooth operations of the linear compressor.

5. Conclusion

In the present paper, the dynamic characteristics of the DOLC were studied through experimental and theoretical research. The experimental results show that the performance of DOLC was significantly affected by work conditions and stiffness of the syntonic spring groups. The DOLC showed the highest efficiency at sympathetic vibration, but its working status was unstable. The displacement jump or shrink phenomenon will occur when the frequency ratio is near to 1.0; the displacement jump will cause the discharge pressure to drop. Because sympathetic vibration conditions were different from discharge pressures, a hysteresis district between the displacement jump point and shrink point existed. The DOLC worked in a stable manner on the hysteresis district because of discharge pressure fluctuations. To ensure that the DOLC will work steadily to achieve higher efficiency, the intrinsic frequency must be configured to a slightly larger value than the power frequency. This can be achieved by setting the syntonic spring groups and movement component mass according to the rating work conditions. Moreover, the power frequency should be controlled to adhere to the intrinsic frequency on variable work conditions.

Acknowledgment

The work was supported by a grant (No. 2007AA05Z258) from the National High Technology Research and Development Program of China (863 Program).

References

[1] C. Minas, Nonlinear dynamics of an oilless linear drive reciprocating compressor, *Journal of Vibration and Acoustics*, *ASME* (1994) 79-84.

[2] G. Choe and K. Kim, Analysis of nonlinear dynamics in a linear compressor, *International Journal Series C of Japan Society of Mechanical Engineers* (2000) 545-552.

[3] G. Choe and K. Kim, Theoretical and experimental analysis of nonlinear dynamics in a linear compressor, *Journal of Vibration and Acoustics*, *ASME* (2002) 152-156.

[4] M. Lamantia, A. Contarini and S. Giovanni, Numerical and experimental analysis of a linear compressor, In: *Proceedings of International compressor Engineering Conference at Purdue, Purdue University* (2002) 554-561.

[5] N. Chen, Y. Tang and Y. Wu, Study on static and dynamic characteristics of moving magnet linear compressors, *Cryogenics* (2007) 457-467.

[6] H. Kim, C. Roh, J. Kim, J. Shin, Y. Hwang and J. Lee, An experimental and numerical study on dynamic characteristic of linear compressor in refrigeration system, *International Journal of Refrigeration* (2009) 1536-1542.

[7] R. Redlich, R. Unger and N. Walt, Linear compressor: moter configuration, modulation and systems, *International Compressor Engineering Conference, Purdue University* (1996).

[8] Y. Z. Yu, Technology manual of Displacement compressor, *Machinery Industry Press* (2000) 38-48 (In chinese).

Appendix

The work cycle of the reciprocating compressor is generally regarded as a constant-quality polytropic process when heat transfer and flow leakage are considered. Polytropic process index n can be corrected from the adiabatic index κ, i.e., (0.93~0.98)κ [8]. The ratio of the amplitude of piston displacement X and the clearance distance X_0 determine the output of the work cycle.

If $\frac{X}{X_0} > \frac{p_d^{1/n} - p_s^{1/n}}{p_d^{1/n} + p_s^{1/n}}$, the compressor will be pumping gas.

If $\frac{X}{X_0} \le \frac{p_d^{1/n} - p_s^{1/n}}{p_d^{1/n} + p_s^{1/n}}$, the compressor will not be pumping gas.

Fig. A.1 shows the changes in the gas force with the displacement in a cycle of pumping gas. The gas force of the DOLC can be described as follows:

(1) From 0 to θ_1, cylinder 1 is in the process of polytropic compression and cylinder 2 is in the process of constant pressure suction. In these processes, the gas force can be expressed by:

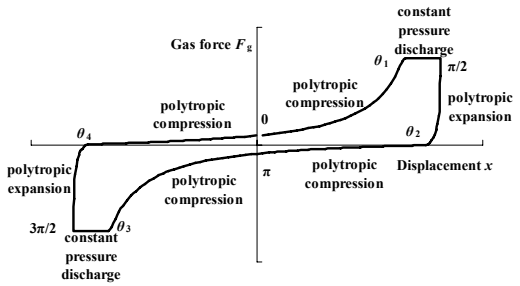

Fig. A.1. Changes in the gas force curves with the displacement of pumping cycle.

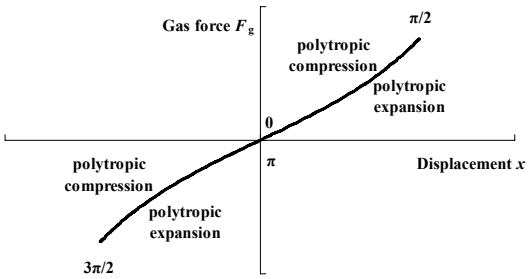

Fig. A.2. Changes in the gas force curves with the displacement of the no pumping cycle.

$$F_g = p_s A\left[(\frac{X_0 + X}{X_0 - x})^n - 1 \right].$$

(2) From θ_1 to $\pi/2$, cylinder 1 is in the process of constant pressure discharge and cylinder 2 is in the process of constant pressure suction. In these processes, the gas force can be expressed by:

$$F_g = (p_d - p_s)A.$$

(3) From $\pi/2$ to θ_2, cylinder 1 is in the process of polytropic expansion and cylinder 2 is in the process of polytropic compression. In these processes, gas force can be expressed by:

$$F_g = A\left[(\frac{X_0 - X}{X_0 - x})^n p_d - (\frac{X_0 + X}{X_0 + x})^n p_s \right].$$

(4) From θ_2 to π, cylinder 1 is in the process of constant pressure suction and cylinder 2 is in the process of polytropic compression. In these processes, the gas force can be expressed by:

$$F_g = Ap_s\left[1 - (\frac{X_0 + X}{X_0 + x})^n \right].$$

(5) From π to θ_3, cylinder 1 is in the process of constant pressure suction and cylinder 2 is in the process of constant pressure discharge. In these processes, the gas force can be expressed by:

$$F_g = (p_s - p_d)A.$$

(6) From θ_3 to $3\pi/2$, cylinder 1 is in the process of polytropic compression and cylinder 2 is in the process of polytropic expansion. In these processes, the gas force can be expressed by:

$$F_g = A\left[(\frac{X_0 + X}{X_0 - x})^n p_d - (\frac{X_0 - X}{X_0 + x})^n p_s \right].$$

(7) From $3\pi/2$ to θ_4, cylinder 1 is in the process of polytropic compression and cylinder 2 is in the process of constant pressure suction. In these processes, the gas force can be expressed by:

$$F_g = p_s A\left[(\frac{X_0 + X}{X_0 - x})^n - 1 \right]$$

where n is the polytropic process index corrected from the gas adiabatic index κ, p_d is the discharge pressure (MPa), p_s is the suction pressure (MPa), θ_1 is the angular position at the beginning of discharge of one side, θ_2 is the angular position at the end of expansion of one side, θ_3 is the angular position at the beginning of the discharge of the other side, and θ_4 is the angular position at the end of expansion of the other side. They are determined by the amplitude of the piston stroke and can be expressed by:

$$\theta_1 = \arcsin\left[\frac{X_0}{X}\left(\left(\frac{p_s}{p_d} \right)^{1/n} \left(1 + \frac{X}{X_0} \right) - 1 \right) \right]$$

$$\theta_2 = \pi - \arcsin\left[\frac{X_0}{X}\left(\left(\frac{p_d}{p_s} \right)^{1/n} \left(1 - \frac{X}{X_0} \right) - 1 \right) \right]$$

$$\theta_3 = \pi + \theta_1,\ \ \theta_3 = \pi + \theta_2.$$

Fig. 2 shows the changes in the gas force with the displacement in the no pumping gas cycle. The gas force of the DOLC can be described as follows:

(1) From 0 to $\pi/2$, cylinder 1 is in the process of polytropic compression and cylinder 2 is in the process of polytropic expansion. In these processes, the gas force can be expressed by:

$$F_g = Ap_s\left[(\frac{X_0 + X}{X_0 + x})^n - (\frac{X_0 + X}{X_0 + x})^n (\frac{X_0 - X}{X_0 - x})^n \right].$$

(2) From $\pi/2$ to $3\pi/2$, cylinder 1 is in the process of polytropic expansion and cylinder 2 is in the process of polytropic compression. In these processes, the gas force can be expressed by:

$$F_g = Ap_s\left[(\frac{X_0 + X}{X_0 - x})^n (\frac{X_0 - X}{X_0 - x})^n - (\frac{X_0 + X}{X_0 + x})^n \right].$$

(3) From $3\pi/2$ to 2π, cylinder 1 is in the process of polytropic compression and cylinder 2 is in the process of polytropic expansion. In these processes, the gas force can be expressed by:

$$F_g = Ap_s\left[(\frac{X_0+X}{X_0+x})^n - (\frac{X_0+X}{X_0+x})^n(\frac{X_0-X}{X_0-x})^n\right].$$

Because of the nonlinear feature of gas force, directly analyzing the dynamic characteristics of the DOLC with the above gas force expression is difficult. To simplify the analysis, linearizing the gas force by Fourier transformation is necessary. The gas force of the DOLC can be linearized into the following formula by the one-order Fourier transformation [2]. The equivalent gas force F_{eg} can be expressed as:

$$F_{eg} = a_1\cos\omega t + b_1\sin\omega t + F_s\,. \tag{A.1}$$

For the pumping cycle:

$$\begin{aligned}
a_1(X,X_0) &= \frac{1}{\pi}\int_0^{2\pi} F_g(t)\cos\omega t d(\omega t)\\
&= \frac{Ap_s}{\pi}\int_0^{\theta_1}\left[(\frac{X_0+X}{X_0-X\sin\omega t})^n - 1\right]\cos\omega t d(\omega t) + \frac{A}{\pi}\int_{\theta_1}^{\frac{\pi}{2}}(p_d-p_s)\cos\omega t d(\omega t)\\
&+ \frac{A}{\pi}\int_{\frac{\pi}{2}}^{\theta_2}\left[(\frac{X_0-X}{X_0-X\sin\omega t})^n p_d - (\frac{X_0+X}{X_0+X\sin\omega t})^n p_s\right]\cos\omega t d(\omega t)\\
&+ \frac{Ap_s}{\pi}\int_{\theta_2}^{\theta_3}\left[1-(\frac{X_0+X}{X_0+X\sin\omega t})^n\right]\cos\omega t d(\omega t) + \frac{A}{\pi}\int_{\theta_3}^{\frac{3\pi}{2}}(p_s-p_d)\cos\omega t d(\omega t)\\
&+ \frac{A}{\pi}\int_{\frac{3\pi}{2}}^{\theta_4}\left[(\frac{X_0+X}{X_0-X\sin\omega t})^n p_s - (\frac{X_0-X}{X_0+X\sin\omega t})^n p_d\right]\cos\omega t d(\omega t)\\
&+ \frac{Ap_s}{\pi}\int_{\theta_4}^{2\pi}\left[(\frac{X_0+X}{X_0-X\sin\omega t})^n - 1\right]\cos\omega t d(\omega t)\\
b_1(X,X_0) &= \frac{1}{\pi}\int_0^{2\pi} F_g(t)\sin\omega t d(\omega t)\\
&= \frac{Ap_s}{\pi}\int_0^{\theta_1}\left[(\frac{X_0+X}{X_0-X\sin\omega t})^n - 1\right]\sin\omega t d(\omega t) + \frac{A}{\pi}\int_{\theta_1}^{\frac{\pi}{2}}(p_d-p_s)\sin\omega t d(\omega t)\\
&+ \frac{A}{\pi}\int_{\frac{\pi}{2}}^{\theta_2}\left[(\frac{X_0-X}{X_0-X\sin\omega t})^n p_d - (\frac{X_0+X}{X_0+X\sin\omega t})^n p_s\right]\sin\omega t d(\omega t)\\
&+ \frac{Ap_s}{\pi}\int_{\theta_2}^{\theta_3}\left[1-(\frac{X_0+X}{X_0+X\sin\omega t})^n\right]\sin\omega t d(\omega t) + \frac{A}{\pi}\int_{\theta_3}^{\frac{3\pi}{2}}(p_s-p_d)\sin\omega t d(\omega t)\\
&+ \frac{A}{\pi}\int_{\frac{3\pi}{2}}^{\theta_4}\left[(\frac{X_0+X}{X_0-X\sin\omega t})^n p_s - (\frac{X_0-X}{X_0+X\sin\omega t})^n p_d\right]\sin\omega t d(\omega t)\\
&+ \frac{Ap_s}{\pi}\int_{\theta_4}^{2\pi}\left[(\frac{X_0+X}{X_0-X\sin\omega t})^n - 1\right]\sin\omega t d(\omega t)\\
F_s(X,X_0) &= \frac{1}{2\pi}\int_0^{2\pi} F_g(t)d(\omega t)\\
&= \frac{Ap_s}{2\pi}\int_0^{\theta_1}\left[(\frac{X_0+X}{X_0-X\sin\omega t})^n - 1\right]d(\omega t) + \frac{A}{2\pi}\int_{\theta_1}^{\frac{\pi}{2}}(p_d-p_s)d(\omega t)\\
&+ \frac{A}{2\pi}\int_{\frac{\pi}{2}}^{\theta_2}\left[(\frac{X_0-X}{X_0-X\sin\omega t})^n p_d - (\frac{X_0+X}{X_0+X\sin\omega t})^n p_s\right]d(\omega t)\\
&+ \frac{Ap_s}{2\pi}\int_{\theta_2}^{\theta_3}\left[1-(\frac{X_0+X}{X_0+X\sin\omega t})^n\right]d(\omega t) + \frac{A}{2\pi}\int_{\theta_3}^{\frac{3\pi}{2}}(p_s-p_d)d(\omega t)\\
&+ \frac{A}{2\pi}\int_{\frac{3\pi}{2}}^{\theta_4}\left[(\frac{X_0+X}{X_0-X\sin\omega t})^n p_s - (\frac{X_0-X}{X_0+X\sin\omega t})^n p_d\right]d(\omega t)\\
&+ \frac{Ap_s}{2\pi}\int_{\theta_4}^{2\pi}\left[(\frac{X_0+X}{X_0-X\sin\omega t})^n - 1\right]d(\omega t)\,.
\end{aligned}$$

For the no pumping cycle:

$$\begin{aligned}
a_1(X,X_0) &= \frac{1}{\pi}\int_0^{2\pi} F_g(t)\cos\omega t d(\omega t)\\
&= \frac{Ap_s}{\pi}\int_0^{\frac{\pi}{2}}\left[(\frac{X_0+X}{X_0-X\sin\omega t})^n - (\frac{X_0-X}{X_0+X\sin\omega t})^n(\frac{X_0+X}{X_0-X\sin\omega t})^n\right]\cos\omega t d(\omega t)\\
&+ \frac{Ap_s}{\pi}\int_{\frac{\pi}{2}}^{\frac{3\pi}{2}}\left[(\frac{X_0-X}{X_0-X\sin\omega t})^n(\frac{X_0+X}{X_0-X\sin\omega t})^n - (\frac{X_0+X}{X_0+X\sin\omega t})^n\right]\cos\omega t d(\omega t)\\
&+ \frac{Ap_s}{\pi}\int_{\frac{3\pi}{2}}^{2\pi}\left[(\frac{X_0+X}{X_0-X\sin\omega t})^n - (\frac{X_0-X}{X_0+X\sin\omega t})^n(\frac{X_0+X}{X_0-X\sin\omega t})^n\right]\cos\omega t d(\omega t)\\
b_1(X,X_0) &= \frac{1}{\pi}\int_0^{2\pi} F_g(t)\sin\omega t d(\omega t)\\
&= \frac{Ap_s}{\pi}\int_0^{\frac{\pi}{2}}\left[(\frac{X_0+X}{X_0-X\sin\omega t})^n - (\frac{X_0-X}{X_0+X\sin\omega t})^n(\frac{X_0+X}{X_0-X\sin\omega t})^n\right]\sin\omega t d(\omega t)\\
&+ \frac{Ap_s}{\pi}\int_{\frac{\pi}{2}}^{\frac{3\pi}{2}}\left[(\frac{X_0-X}{X_0-X\sin\omega t})^n(\frac{X_0+X}{X_0-X\sin\omega t})^n - (\frac{X_0+X}{X_0+X\sin\omega t})^n\right]\sin\omega t d(\omega t)\\
&+ \frac{Ap_s}{\pi}\int_{\frac{3\pi}{2}}^{2\pi}\left[(\frac{X_0+X}{X_0-X\sin\omega t})^n - (\frac{X_0-X}{X_0+X\sin\omega t})^n(\frac{X_0+X}{X_0-X\sin\omega t})^n\right]\sin\omega t d(\omega t)\\
F_s(X,X_0) &= \frac{1}{2\pi}\int_0^{2\pi} F_g(t)d(\omega t)\\
&= \frac{Ap_s}{2\pi}\int_0^{\frac{\pi}{2}}\left[(\frac{X_0+X}{X_0-X\sin\omega t})^n - (\frac{X_0-X}{X_0+X\sin\omega t})^n(\frac{X_0+X}{X_0-X\sin\omega t})^n\right]d(\omega t)\\
&+ \frac{Ap_s}{2\pi}\int_{\frac{\pi}{2}}^{\frac{3\pi}{2}}\left[(\frac{X_0-X}{X_0-X\sin\omega t})^n(\frac{X_0+X}{X_0-X\sin\omega t})^n - (\frac{X_0+X}{X_0+X\sin\omega t})^n\right]d(\omega t)\\
&+ \frac{Ap_s}{2\pi}\int_{\frac{3\pi}{2}}^{2\pi}\left[(\frac{X_0+X}{X_0-X\sin\omega t})^n - (\frac{X_0-X}{X_0+X\sin\omega t})^n(\frac{X_0+X}{X_0-X\sin\omega t})^n\right]d(\omega t).
\end{aligned}$$

The gas force of the DOLC is symmetrical. Thus, $F_s(X,X_0)=0$. The gas force can be linearized using formula (A.2)

$$F_{eg} = k_g x + c_g\frac{dx}{dt} \tag{A.2}$$

where c_g is the gas equivalent damping coefficient and k_g is the gas equivalent stiffness coefficient. Both can be expressed by:

$$k_g = \frac{a_1(X,X_0)}{X} \tag{A.3}$$

$$c_g = \frac{b_1(X,X_0)}{\omega X}\,. \tag{A.4}$$

Huiming Zou was born in China in 1977. She received a Ph.D. in Cryogenics and Refrigeration Engineering in 2010. She currently works as an Assistant Researcher in Technical institute of Physics and Chemistry, CAS. Her research interests include new technologies for refrigeration and HVAC system.